

The reconstruction of water table depth over the past 3100 years in south-eastern Australia using testate amoebae and potential implications for Pacific climatic variability

Xianglin Zheng ^a, Geoffrey Hope ^b, Scott D. Mooney ^{a,*}

^a School of Biological, Earth & Environmental Sciences, UNSW, Sydney, Australia

^b Department of Archaeology and Natural History, Australian National University, Australia

ARTICLE INFO

Editor: Howard Falcon-Lang

Keywords:

Bog
Rainfall
Climate variability
ENSO

ABSTRACT

Due to the temperate and relatively dry climate of south-eastern Australia, there are relatively few moisture-sensitive palaeoenvironmental records in the region. The region is of significance as it is influenced by several major ocean-atmospheric modes including El Niño–Southern Oscillation (ENSO) and the Inter-decadal Pacific Oscillation (IPO). In this research we applied a transfer function between (sub)fossil testate amoebae and water table depth to consider local surface wetness, which may reflect effective moisture conditions, at Snowy Flat, a high-altitude *Sphagnum*-shrub bog in south-eastern Australia over the late Holocene. The reconstruction water table depth, covering the last ~3100 cal yr B.P., suggested several distinct periods of enhanced surface wetness, perhaps reflecting moisture availability, including from 2400 to 2200, 1350–1100, 920–860 and 670 to 60 cal yr B.P.. After 1800 cal yr B.P., depth to water table (DWT) was more variable and followed well-known trends of the Northern Hemisphere including the Medieval Climatic Anomaly (MCA; increased DWT) and the Little Ice Age (LIA; decreased DWT). We also investigated the instrumental record of rainfall and found a significant negative relationship with the IPO and an IPO-like tripole spatial pattern between rainfall and sea surface temperatures in the Pacific Ocean. This suggests that the late Holocene hydroclimate at the Snowy Flat site, and across south-eastern Australia and more widely, can be related to the IPO and this is especially true after 1800 cal yr B.P. when the relationship apparently strengthened. The reconstruction also indicated that a positive IPO (El Niño-like) mean state prevailed in the MCA and a negative IPO (La Niña-like) mean state dominated the LIA. Surface moisture (DWT) was also related to total solar irradiance (from ¹⁰Be in polar ice): periods of enhanced surface moisture (reduced DWT) (mean negative IPO states) coincided with minima (e.g. 920–860 and 670–60 ca. yr B.P.) and reduced moisture (increased DWT) coincided with maxima (e.g. 850–700 cal yr B.P.). Together these results shed further light on the variability of moisture in south-eastern Australia, and further afield, and the potential mechanisms for these.

1. Introduction

The scarcity of palaeoenvironmental reconstruction in the Southern Hemisphere has led to a bias in global syntheses considering the Holocene (Wanner et al., 2015; Jansen et al., 2007) and this is also true for the late Holocene (PAGES 2k Consortium, 2013; Mann et al., 2009; Neukom and Gergis, 2012). This is despite the fact that some Southern Hemisphere regions are under the influence of several major ocean-atmospheric modes: as an example, south-eastern Australia is located in the core area of the El Niño–Southern Oscillation (ENSO) and the Interdecadal Pacific Oscillation (IPO) (Risbey et al., 2009; Henley et al.,

2011; Power et al., 1999). These sources of variability impact both hemispheres and through teleconnections, a wide geographic extent. They may also be sensitive to future climate change.

This means that any novel palaeoenvironmental reconstruction that offers insight to the climate system in south-eastern Australia may be applicable to ocean-atmospheric modes that operate at much larger spatial scales. The relatively dry climate of south-eastern Australia means that many palaeoenvironmental archives (and proxies) widely-used in other locations, such as tree rings or lake sediments, are rare or not available in the region (Barr et al., 2014). As an example, using these two widely used sources of palaeohydrological information,

* Corresponding author.

E-mail address: s.mooney@unsw.edu.au (S.D. Mooney).

permanent or semi-permanent lakes are rare in eastern Australia (Chang et al., 2014), with the exception of Tasmania, and long-lived, sensitive trees are also largely confined to Tasmania (Palmer et al., 2015; Heinrich and Allen, 2013).

This means that Australia has relatively few palaeoenvironmental records that have particularly focused on palaeohydrology (Petherick et al., 2013; Gouramanis et al., 2013), and quantitative reconstructions are even rarer (Zheng et al., 2019a). As a consequence, those that are available have been influential, and this includes the Holocene water level curve derived from Lake Keilambete (Bowler, 1981) and from the south-western Victorian region (Wilkins et al., 2013; Barr et al., 2014).

Mires, a collective term for various wetlands, including bogs, fens and swamps (Gore, 1983; Whinam and Hope, 2005), are intrinsically related to hydrology via waterlogging, anoxia and hence the accumulation of organic sediments ('peat' formation). The quantification of palaeohydrology of such sites can provide information about past moisture availability, variability and potentially, about climatic drivers.

Testate amoebae have been used extensively in the Northern Hemisphere as a moisture-sensitive proxy (Mitchell et al., 2008; Amesbury et al., 2016; Warner and Charman, 1994) and in the Southern Hemisphere for various purposes (e.g., McKeown et al., 2024; Mieczan and Adamczuk, 2015; van Bellen et al., 2014). The development of a statistical relationship (transfer functions) between the modern community composition of testate amoeba and water table depth (WTD) allows, for example, the quantification of past surface wetness and hence water balance and palaeohydrological variability, particularly in ombrotrophic bogs. Despite this potential, testate amoebae have not been tested and applied to the consideration of palaeo-hydrology in Australia.

This study uses a transfer function linking testate amoebae community composition and WTD (Zheng et al., 2019a) at a high-altitude mire in south-eastern Australia over the late Holocene. Our aim was to reconstruct past WTD as a proxy for local surface wetness, which may reflect effective moisture conditions, to consider the nature and sources of palaeo-hydrological variability.

2. Site description and methods

2.1. Site description

Snowy Flat bog (35.5628° S, 148.7837° E) is a *Sphagnum-Richea-Empodium* shrub bog of approximately 20.5 ha in size, located at 1609 m asl in the Australian Capital Territory (ACT) (Fig. 1). The vegetation of Snowy Flat is dominated by *Richea continentis*, *Empodium minus* and *Sphagnum cristatum*, with scattered occurrences of *Epacris paludosa*, *Epacris brevifolia* and *Baloskion australis*.

Snowy Flat experiences a subalpine climate, which is inferred from an automatic weather station 4 km away near Mount Ginini over the period of 2014 and 2018 (BOM, 2018a). The total mean annual rainfall is 1051 mm, with an almost uniform rainfall regime falling in both the warmer (December–May) and cooler months (June–November). The mean maximum temperature is 11.7° C, and this ranges from a minimum in July of 2.0° C to a maximum in January of 21.0° C. The mean minimal temperature is 3.5° C, ranging from a low of -2.7° C in July to 10° C in January.

The site is best characterized as a topogenous bog occupying the base of a broad valley floor and this valley includes some small channelised water flows (Hope, 2003; Hope et al., 2009). Ground water flows are largely unexplored although Muller et al. (2016) argued that groundwater is not a major part of the hydrology of the Snowy Flat Bog. Our observations support the contention that groundwater flows are likely only to affect the hydrology of the edges of Snowy Flat Bog. *Sphagnum*-dominated patches on the bog are often raised and hence have an ombrotrophic-like nature.

2.2. The instrumental record of rainfall

The longest instrumental record of meteorological data close to the Snowy Flat bog is approximately 50 km to the south at the Adaminaby Alpine Tourist Park (BOM station number: 71000, BOM, 2018b). This

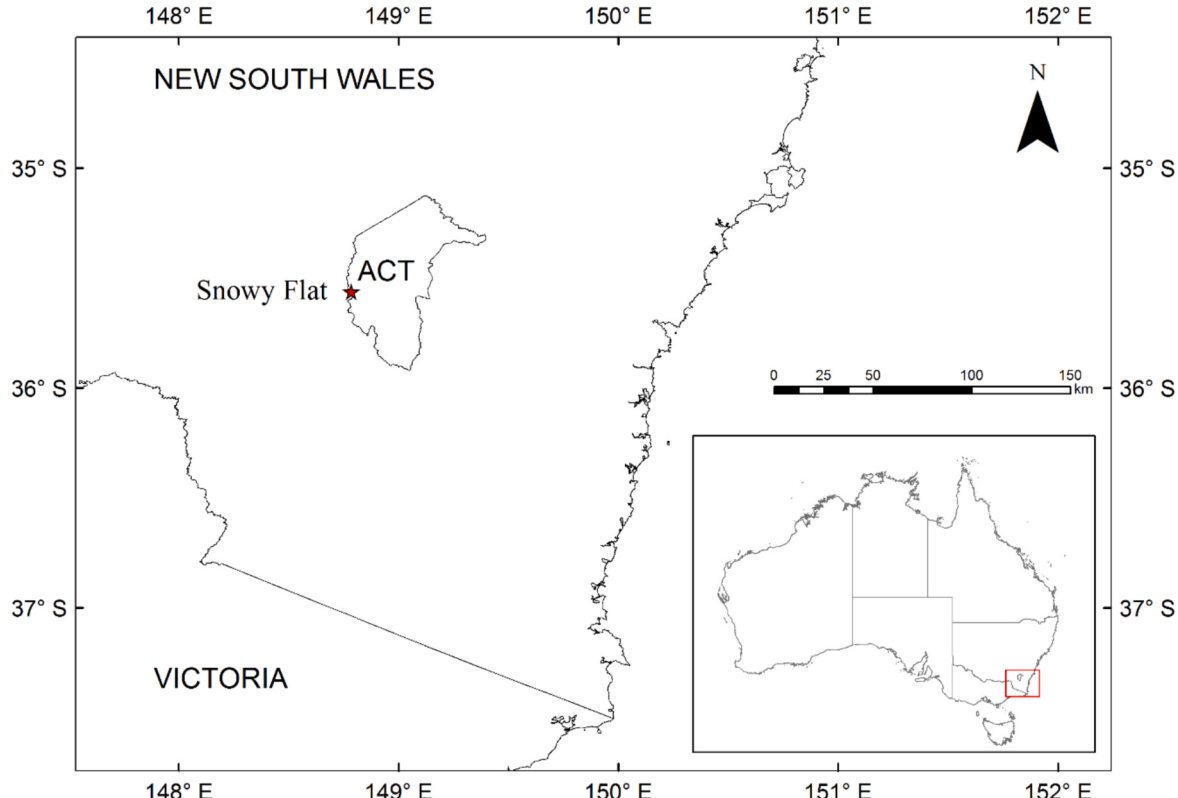


Fig. 1. Location of Snowy Flat in south-eastern Australia. ACT refers to the Australian Capital Territory.

station is located at lower altitude (1015 m cf. Snowy Flat at 1605 m asl) but rainfall at the two stations is significantly correlated during the period of overlap (Pearson Correlation coefficient $r = 0.77$, $P < 0.001$).

To consider the decadal variability in the Adaminaby record we calculated rainfall anomalies (using LOESS with span = 0.75 and degree = 2 in R) and this data were smoothed with an 85-month moving average, twice, following Dai (2013). In south-eastern Australia Power et al. (1999) suggested that rainfall is modulated by the IPO: more recent analyses by Risbey et al. (2009) demonstrated that under a negative IPO there is a significant positive relationship between La Niña and rainfall, but this is not the case under a positive IPO. Based on this, we compared the smoothed anomaly Adaminaby rainfall record and the IPO tripole index (TPI) which is based on the NOAA ERSSTv4 (Henley et al., 2015). For this comparison we smoothed the TPI in the same way as the rainfall anomaly.

To consider how the rainfall at the site fits into the climate of the region and more broadly, we examined the correlation between annual rainfall at Adaminaby and detrended annual rainfall (CRU TS 4.01: Peterson and Vose, 1997) and detrended annual sea surface temperature (SST) (HadISST 1.1: Rayner et al., 2003) over the period of 1887 to 1989 in the circum-Pacific region (from 100°E to 60°W). These analyses were conducted using the KNMI Climate Explorer (available at <http://climexp.knmi.nl>: van Oldenborgh and Burgers, 2005).

2.3. Sediment sampling

Cores of more consolidated sediments were retrieved from a hummock (35.5628°S, 148.7837°E) on 15th December 2016 with a D-section corer (Jowsey, 1966), covering the depths from 110 to 267 cm (with 5 cm overlap between adjacent cores, e.g. 110–150 cm and 145–195 cm). The upper, less consolidated materials proved difficult to sample with the D-section corer and hence three monoliths were sampled (in February 2018) from a hummock approximately 1.5 m to the west of the previous cores using a saw. These were sampled in three sections: 0–45, 35–78 and 70–106 cm in depth. At the time of retrieving the upper monoliths, the WTD was 70 cm. This resulted in samples from Snowy Flat covering from the surface to a depth 267 cm. The sediment cores were carefully wrapped in the field with plastic film and aluminium foil and secured into plastic cradles for transport. The cores were then placed in refrigerated storage (at 4 °C) in sealed plastic containers in an attempt to minimize oxidation.

2.4. Sediment chronology

Short-lived plant macro-fossils or in their absence, large ($>250 \mu\text{m}$) pieces of charcoal were wet sieved from nine narrow depths of the sediment column for Accelerator Mass Spectrometry (AMS) radiocarbon (^{14}C) dating. The SHCal13 curve (Hogg et al., 2013) was used in the calibration of these radiocarbon ages. In addition, the first appearance of the pollen of the exotic genus *Pinus* at 105 cm in the upper monoliths was used to approximate the time of European arrival. There is some uncertainty as to whether the first appearance of *Pinus* represents the first non-Indigenous settlement or the first Pine plantations in the region (e.g. see Tibby, 2003) and hence we conservatively estimated this as 50 ± 30 yr B.P. (1900 CE with a range of 1870 to 1930). An age-depth model was then developed using ‘Bacon’ which uses a Bayesian, hierarchical model with autoregressive gamma processes (Blaauw and Christen, 2011). In this research, the surface sample at 0 cm was set as the sampling year with a 1-year error to constrain the starting point.

2.5. Testate amoebae

(Sub)fossil testate amoebae were quantified in both the upper material recovered in the monolith sections (0–106 cm) and from the D-section cores (110–267 cm). Within the upper sediments 8 samples were analysed from relatively wide sections (0–10 cm, 25–30 cm, 50–52 cm,

70–72 cm, 80–82 cm, 90–92 cm, 99–101 cm and 104–106 cm): this strategy was chosen as this material was less consolidated and likely to have accumulated relatively quickly. Within the deeper sediments 0.5 cm wide sections were taken at a 3-cm interval from the depth of 110 cm to 221 cm. Preliminary analysis demonstrated that the abundance of testate amoebae generally reduced with depth in the cores, making their quantification challenging and time-consuming. In addition, two extra samples were processed and quantified at depths representing 210.5 cm and 213.5 cm: these were added later, to assess preliminary trends. This resulted in a total of 48 samples analysed between a depth of 0 cm and 221 cm at Snowy Flat.

Testate amoebae were prepared using 3.0 cm^3 of sediment, following the method described for minerogenic sediments by Zheng et al. (2019b), and this differs from standard protocols (Booth et al., 2010) with the addition of a dispersant (sodium pyrophosphate) and acetone into the mild (NaOH) alkaline treatments. *Lycopodium* spores were also added to keep track of the volume of material considered. At least 50 individual testate amoebae were counted for each depth sample but counting stopped once the number of added *Lycopodium* spores exceeded 200. Fifty individual testate amoebae are statistically robust for the reconstruction of WTD (Payne and Mitchell, 2009). Testate amoebae identification followed Sullivan and Booth (2007) which was based on Charman et al. (2000), and Southern Hemisphere endemic taxa were identified using Patagonian references (van Bellen et al., 2014).

2.6. Numerical methods

WTD reconstruction was derived from transfer functions that were developed and tested in the region (Zheng et al., 2019a). That work demonstrated that the modern analogue technique (MAT) had the best overall (statistical) performance, followed by a method using weighted average with classical de-shrinking (WA.cl). Although a Gaussian logit regression with maximum likelihood calibration model (ML) was found to have a poorer performance, it is used here for comparison.

Numeric analysis was undertaken in R using ‘rioja’ (Juggins, 2017) and ‘vegan’ (Oksanen et al., 2015). Relative concentration was calculated using the known concentration of *Lycopodium* spores, rather than using volumetric concentration. To consider the relatedness between samples and to derive zones, constrained incremental sum of squares (CONISS) was completed in the ‘rioja’ package. To emphasize trends, rather than the magnitude of change, Charman et al. (2006) and Swindles et al. (2015) recommended using z-scores of WTD and hence the reconstructed WTD from the transfer models was detrended and normalized using z-scores. Graphical outputs were completed using ‘ggplot2’ (Wickham, 2009) and ‘rioja’. Monte Carlo resampling was used to derive an empirical distribution of dissimilarity via resampling pair-wise dissimilarity in the modern training samples (Birks et al., 2012). The minimum dissimilarity among the dissimilarities between one (sub)fossil sample and all modern training samples was used to represent the analogue goodness of modern sample for that (sub)fossil sample.

3. Results

3.1. Chronology of sedimentation

The radiocarbon results are shown in Table 1. The three radiocarbon results below 236 cm all exceed about 7500 cal yr B.P. whereas the upper 5 are relatively young (younger than ~ 3780 cal yr B.P.). These data suggest either an extremely low rate of sediment accumulation in between or a potential hiatus (at about 230 cm). Notably, a low accumulation rate or hiatus in the growth of peat during the period from ~ 7700 to ~ 3700 cal yr B.P. has been previously identified in highland mires across south-eastern Australia (Dodson, 1987; Cohen and Nanson, 2007; Macphail and Hope, 1985).

To add to the complexity in deriving a chronology for the sediments

Table 1

AMS radiocarbon dating results for Snowy Flat.

Depth (cm)	Materials	Conventional radiocarbon age (yr B.P.)	Calibrated radiocarbon age (cal yr B.P.)	Lab No.
110	Plant macrofossil	109.79 ± 0.41 pMc	(92.9 %) -49 -53 (1.6 %) -9 (0.9 %) -54 (87.4 %) 561-510 626-607 (95.4 %) 961-922 (95.4 %) 1513-1374 (87.5 %) 1826-1698 (7.9 %) 1652-1619 (90.0 %)	β-493,537
115.5–117.5	Charcoal	580 ± 30	561-510 (8.0 %) 626-607 (95.4 %) Wk- 45,361	β-480,584
153–155	Charcoal	1074 ± 19	961-922 (95.4 %) Wk- 45,361	
180–182	Charcoal	1590 ± 19	1513-1374 (95.4 %) 45,362	
202–204	Plant macrofossil	1850 ± 30	1826-1698 (7.9 %) 1652-1619 (90.0 %) 3856-3682 (5.4 %) 3668 - -3642 (95.4 %) 7826-7656 (95.4 %) 7744-7592 (95.4 %) 8170-8019 (95.4 %)	β-493,538
227–229	Charcoal	3530 ± 30	3668 - -3642 (95.4 %) 7826-7656 (95.4 %) 7744-7592 (95.4 %) 8170-8019 (95.4 %)	β-480,587
235–237	Charcoal	6930 ± 30	7826-7656 (95.4 %) Wk- 45,363	β-493,539
243–245	Charcoal	6880 ± 30	7744-7592 (95.4 %) Wk- 45,363	β-480,588
250–252	Charcoal	7324 ± 23	7744-7592 (95.4 %) 8170-8019 (95.4 %)	Wk- 45,363

at Snowy Flat bog, the radiocarbon analysis of the uppermost sample from 110 cm depth suggested that it was a modern sample (with ~110 % modern carbon). As the maximum growth rate of *Sphagnum* in the nearby Ginini Flats Bog, an analogous site, has been determined to approximate 1.8 cm in a growing season, and the net annual growth varied from 0.9 to –0.2 cm (Clark, 1980), a modern age at 110 cm seems exceedingly unlikely. From this it was concluded that that sample was probably contaminated with younger materials from root penetration, and so this age-depth pair was disregarded in the subsequent modelling.

It was difficult for Bacon to adequately model the age-depth relationship at Snowy Flat. Preliminary attempts failed to capture the apparent abrupt change in the mean accumulation rate between the upper sediments (e.g. in the monolith sampled materials) and the more consolidated sediments sampled in the D-section cores. Despite these issues, Bacon uses the advantages of the Bayesian model and takes the accumulation rate of adjacent samples into account and hence was able to build an age-depth model to adequately capture the apparently varying sediment accumulation of Snowy Flat between ~8000 to 570 cal yr B.P.. Due to the uncertainty at the top (e.g. with the apparently contaminated young sample from 110 cm) we applied a simple linear model from the surface to the depth of the first record of the pollen of the exotic genus *Pinus* at a depth of 105 cm (105 cm, 50 ± 30 yr B.P.) and another linear model between this and the next radiocarbon date at 117 cm (β480584) (Fig. 2A).

In the late Holocene the depth-age model derived from Bacon suggests that there were three periods of relatively consistent accumulation at Snowy Flat. Between 3600 and 1800 cal yr B.P., (228 to 204 cm) the accumulation rate at the core site was around 75 yr/cm. After that, between 1800 and 250 cal yr B.P. (from 204 to 110 cm), the accumulation rate approximated 17 yr/cm. In the top section of the (unconsolidated) monolith the accumulation rate was about 1 yr/cm. In this work we report only on analyses in the top 228 cm, representing the last ~3100 cal yr B.P. as this is better constrained by the radiometric dating. Notably, the chronology in this section suggests that the resolution of these analyses (10 cm in the upper core; 0.5 cm in the lower consolidated and humified sediment) represents approximately 5 years.

3.2. (Sub)fossil testate amoebae

A total of 39 unique testate amoebae species were recovered from the Snowy Flat sediments (with all raw data relating to testate amoebae are available online, see Zheng et al., 2025). The number of taxa found in each sample ranged from 6 to 22, with the Shannon Diversity Index (H) indicating species richness ranged from 0.65 to 2.52. The total count ranged from 51 to 119 individuals and the median number of slides analysed was 4, but this ranged to a maximum number of 12, demonstrating the relative scarcity of preserved (sub)fossil testate amoebae in the Snowy Flat sediments.

Fig. 3 displays the spectra of testate amoebae taxa from Snowy Flat against the age of the samples. The most common taxa in the Snowy Flat (sub)fossil samples were *Hyalosphenia subflava*, *Centropyxis platystoma* type, *Certesella martiali*, *Cyclopyxis arcelloides* type and *Assulia muscorum*. From ~3100 to 670 cal yr B.P., the sediment sequence was dominated by *H. subflava* with an average proportion of 42 % across all the samples and from 670 to 60 cal yr B.P. it was dominated by *C. platystoma* type. This transition from *Hyalosphenia subflava* to *Centropyxis platystoma* dominance, at about 670 cal yr BP, may reflect local changes to the substrates as *C. platystoma* prefers inorganic substrates, however loss-on-ignition data (in Zheng, 2018) does not support this. The uppermost sequence, especially after 670 cal yr B.P., generally had a high relative concentration of testate amoeba and a relatively high assemblage abundance (Fig. 3).

3.3. Reconstruction of water table depth

The reconstruction of WTD covered the period from 3100 cal yr B.P. to present. Low WTD describes that the water table is close to the surface, while high WTD reflects a greater depth to the saturated zone. Given that the site of sediment sampling at Snowy Flat Bog was ombrotrophic-like, WTD is largely dependent on surface wetness, precipitation and water balance. Our preliminary threshold for delineating periods of enhanced or reduced WTD was defined as at least 2 data points that exceeded 0.5 in the z-scored data (and hence this represents beyond 0.5 standard deviations).

Fig. 4 shows that the reconstruction of WTD at Snowy Flat using the three transfer functions (MAT, WA.cla and ML) share very similar trends (Fig. 4a). Any discrepancy between these is further reduced using the z-scored WTD (Fig. 4b). As noted in Zheng et al. (2019a) testing of the transfer functions revealed that they are more robust for wet conditions, and hence we are particularly focusing on periods of reduced WTD.

CONISS suggested there were several zones in the Snowy Flat testate amoeba community composition, separated at 1350, 860, 670 and 60 cal yr B.P. (Fig. 3). From 3100 to 1350 cal yr B.P., there were two periods of increased WTD at 2850–2650 and around 1720 cal yr B.P., interspersed by a perhaps wetter period around 2400 cal yr B.P. (Fig. 4b). This period of lower WTD at about 2400 cal yr B.P. was a significant excursion and hence additional data points were placed near this to confirm the trend.

From 1350 to 860 cal yr B.P., there were periods of reduced WTD around 1150 and 920 cal yr B.P., interspersed by what appears to be a relatively drier period around 1040 cal yr B.P.. Although the reduced DTW at around 920 cal yr B.P. and the increased DTW around 1040 cal yr B.P. did not exceed our (0.5 standard deviation) threshold, they show apparent changes compared to adjacent points. From 860 to 670 cal yr B.P., the reconstructed WTD implies a drier water balance but from 670 until 60 cal yr B.P. a relatively wetter period is inferred. After 60 cal yr B.P., a gradually drying trend in the water balance towards the present was suggested.

Fig. 5 shows the reconstructed WTD at Snowy Flat using MAT with the 95 % confidence interval. This figure also shows dissimilarity measures, representing the minimal dissimilarity between a (sub)fossil sample and the modern training samples, which can be considered as an analogue for the goodness of fit between the modern samples and a (sub)

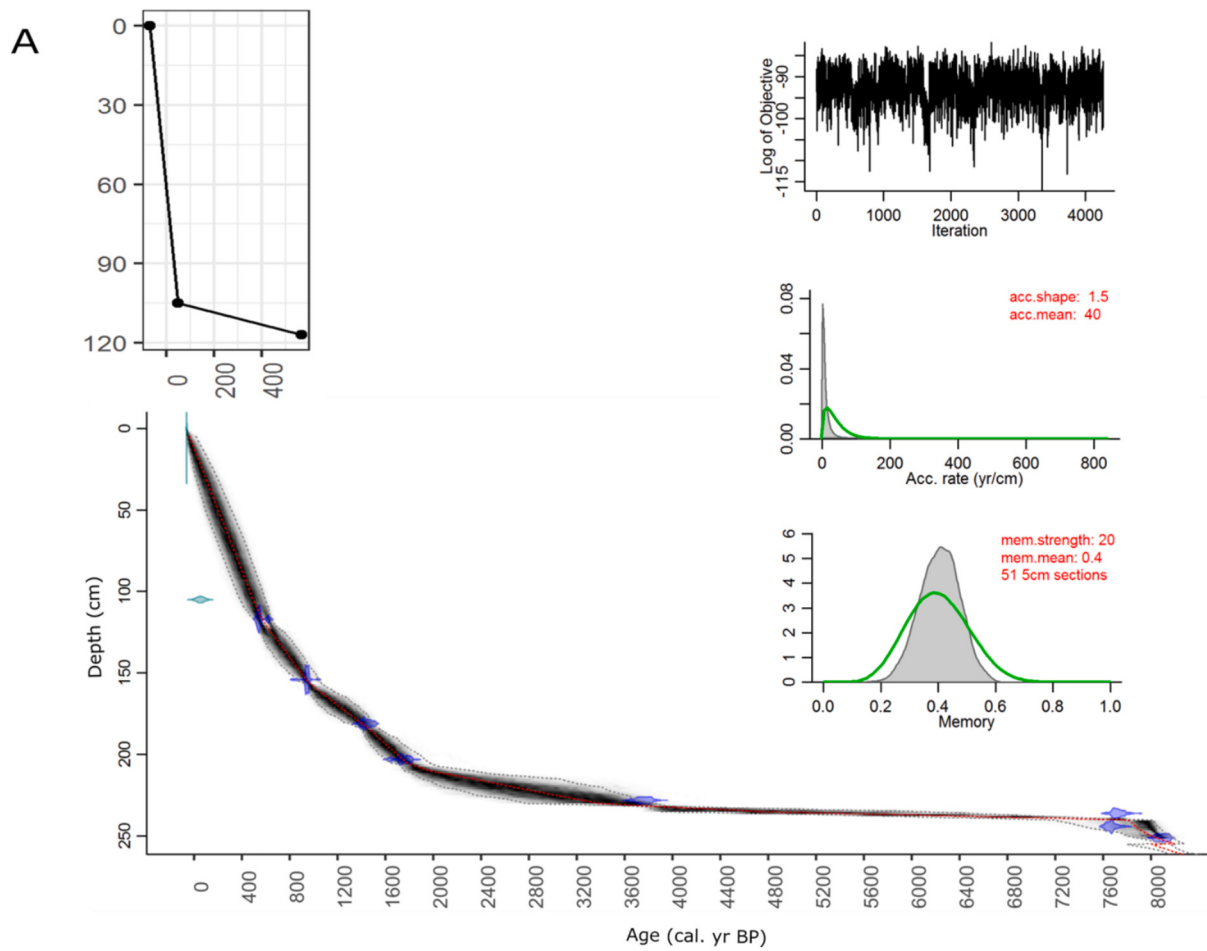


Fig. 2. The age-depth models for the Snowy Flat sediment cores. Inset A shows the age-depth model for the top 117 cm of the sediment. The larger image depicts the age-depth model derived from Bacon. In the right-hand panel, the top graph indicates a convergence of Markov Chain Monte Carlo and in the middle and bottom graphs green lines are prior assumptions and grey areas are posterior distributions. In this research we are only reporting results from the upper 221 cm representing the last 3100 cal yr B.P. (For interpretation of the references to colour in this figure legend, the reader is referred to the web version of this article.)

fossil sample. In the top section of the Snowy Flat core above 130 cm or after 670 cal yr B.P., the dissimilarity quantile generally fell within 10 % but below/prior to this, dissimilarity quantiles exceeded 10 %. Notably, samples from the top section of the D-section cores, from a period of reduced DWT from 670 to 270 cal yr B.P., have very low dissimilarity quantiles (within 2.5 %), indicating concordance with the modern training samples. Consideration of the 95 % confidence intervals for the reconstruction of Snowy Flat WTD using MAT (Fig. 5) also suggests that the suggested period of enhanced water balance from 670 to 270 cal yr B.P. is highly likely to be statistically different to the adjacent period of increased WTD and reduced surface wetness from 870 to 670 cal yr B.P.. The confidence interval also suggests that the period of reduced WTD at 2480 cal yr B.P. was likely to be different to the period of inferred reduced surface wetness at around 2850–2650 cal yr B.P..

3.4. Historic rainfall and modes of variability

In Fig. 6 there is a clear significant negative relationship between the IPO and rainfall in the period prior to 1990 ($r = -0.63 P < 0.001$). This relationship between the IPO and rainfall changed between 1990 and 2005 (to a positive correlation): this change in the IPO has been associated with increasing greenhouse gases (Yeh et al., 2009) or increased aerosols (Hua et al., 2018), but the cause is still unclear. Changes in ENSO ‘flavour’ and relevant atmospheric circulation and teleconnections are also apparent since the 1990s (Yeh et al., 2015; Timermann et al., 2018; Yu et al., 2012). Despite this disturbance, the

relationship was re-established after 2005, and it is probable that the teleconnection represented by the negative correlation between the IPO and rainfall is the dominant, stable configuration back through time.

Fig. 7 shows the correlation between the smoothed rainfall anomaly at Adaminaby and detrended annual rainfall on land in the circum-Pacific land masses. This shows a clear positive correlation between rainfall anomalies at Adaminaby and rainfall across south-eastern Australia. Fig. 7 also reveals a significant correlation between Adaminaby rainfall and SST across the Pacific in a clearly IPO-like tripole pattern. It also demonstrates a weaker but significant ($\alpha = 0.1$) negative correlation with rainfall in land masses of the eastern Pacific, including in the south-western United States of America and southern South America.

4. Discussion

4.1. Reconstruction of water table depth at Snowy flat

The reconstructed WTD from the three transfer function models MAT, WA.cla and ML all revealed extremely similar trends (Fig. 4). The very good agreement between reconstructed WTD from these three models supports the contention that the reconstruction of WTD at Snowy Flat is robust. The top two samples from the depth of 0–5 and 15–30 cm were located within the hummock and the water table depth at the time of sampling was 70 cm, indicating that these surface samples were experiencing relatively dry conditions. The reconstructed WTD (about

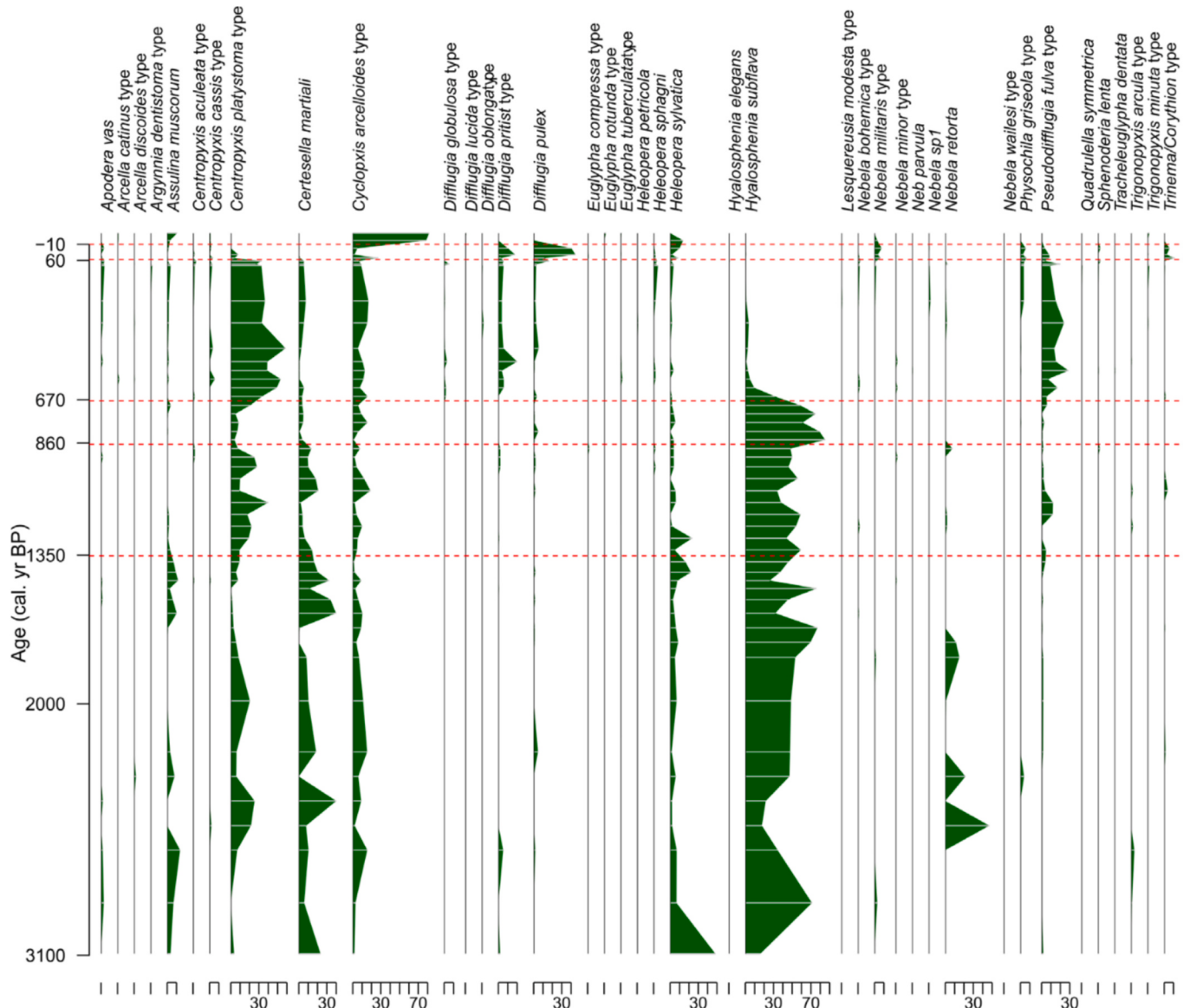


Fig. 3. The spectra of (sub)fossil testate amoebae at Snowy Flat against the age of the samples. The red dashed lines are zone boundaries defined by CONISS. (For interpretation of the references to colour in this figure legend, the reader is referred to the web version of this article.)

45 cm) for these two samples again demonstrates the effectiveness of the developed transfer functions.

Dissimilarity between the (sub)fossil samples and the modern training samples (described in Zheng et al., 2019a) provides another way to consider the goodness of the reconstructed WTD. The (sub)fossil samples after 670 cal yr B.P. had very good modern analogues, and this suggests a high degree of confidence in the performance of the transfer functions in the relatively recent past. This is especially the case for the MAT as that model relies heavily on good analogues with the modern samples. Although the (sub)fossil samples diverged from the modern training samples before 670 cal yr B.P., the reconstructed WTD is still instructive. WA.cla, a transfer function based on weighted averaging, takes the optimal input (WTD) of each taxon into account and derives a weighted average WTD. It is intuitive that when there are abundant taxa in the assemblage who have a 'dry' optimum that this would lead to a relatively high WTD; it hence makes sense the abundance of *H. subflava* before 670 cal yr B.P. resulted in a relatively high WTD (Fig. 3). It should also be emphasised that MAT, WA.cla and ML all gave similar results, even though they use different statistical aspects to approach the reconstruction: this adds confidence to the reconstruction of WTD at

Snowy Flat.

4.2. The reconstruction of WTD at Snowy flat and implications for palaeohydrology in South-Eastern Australia

This work suggests periods of reduced depth to the water table, given the characteristics of the site, probable enhanced water balance around 2480, 1150, 920 cal yr B.P. and between 670 and 60 cal yr B.P.. Periods of increased depth to the water table, and perhaps reduced precipitation have been identified between 2850 and 2650, around 1720, 1040, between 860 and 670 cal yr B.P. and in the very recent past, of approximately the last 60 years (Fig. 4). In contrast to these periods of variability, the reconstruction suggests that the period between about 2200 and 1200 cal yr B.P. was remarkably consistent in terms of surface wetness.

These periods of variability in surface wetness at Snowy Flat have previously been identified in hydroclimatic reconstructions across south-eastern Australia. As an example, the identified periods of reduced WTD around 2480 cal yr B.P. and increased WTD at 1720 cal yr B.P. mirrors the reconstructed lake levels from Lake Keilambete and Lake

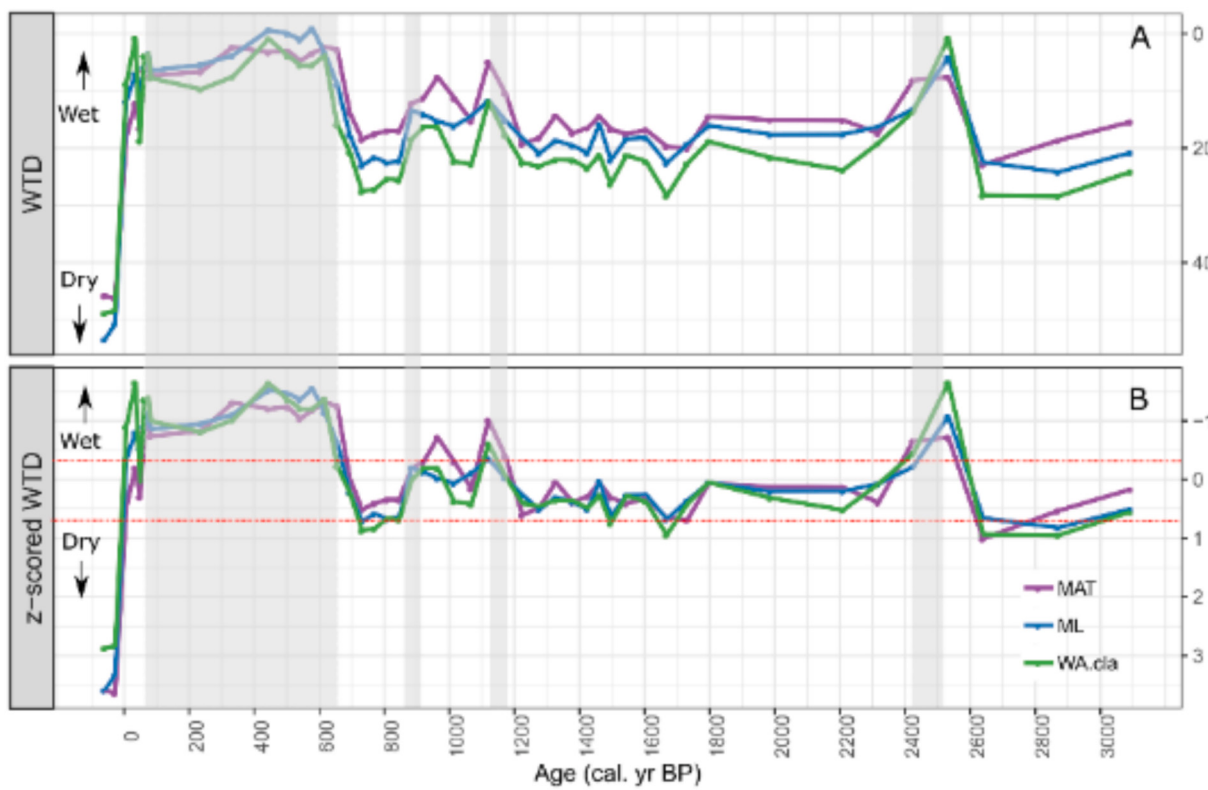


Fig. 4. Panel A (upper) Reconstructed water table depth (WTD) in cm. Panel B (lower) z-scored WTD from Snowy Flat using three different transfer functions (unitless). The grey bars in the background highlight periods when WTD was reduced, reflecting enhanced surface wetness and potentially enhanced precipitation or water balance. The red dashed lines in the lower panel (B) are a threshold at ± 0.5 standard deviations. (For interpretation of the references to colour in this figure legend, the reader is referred to the web version of this article.)

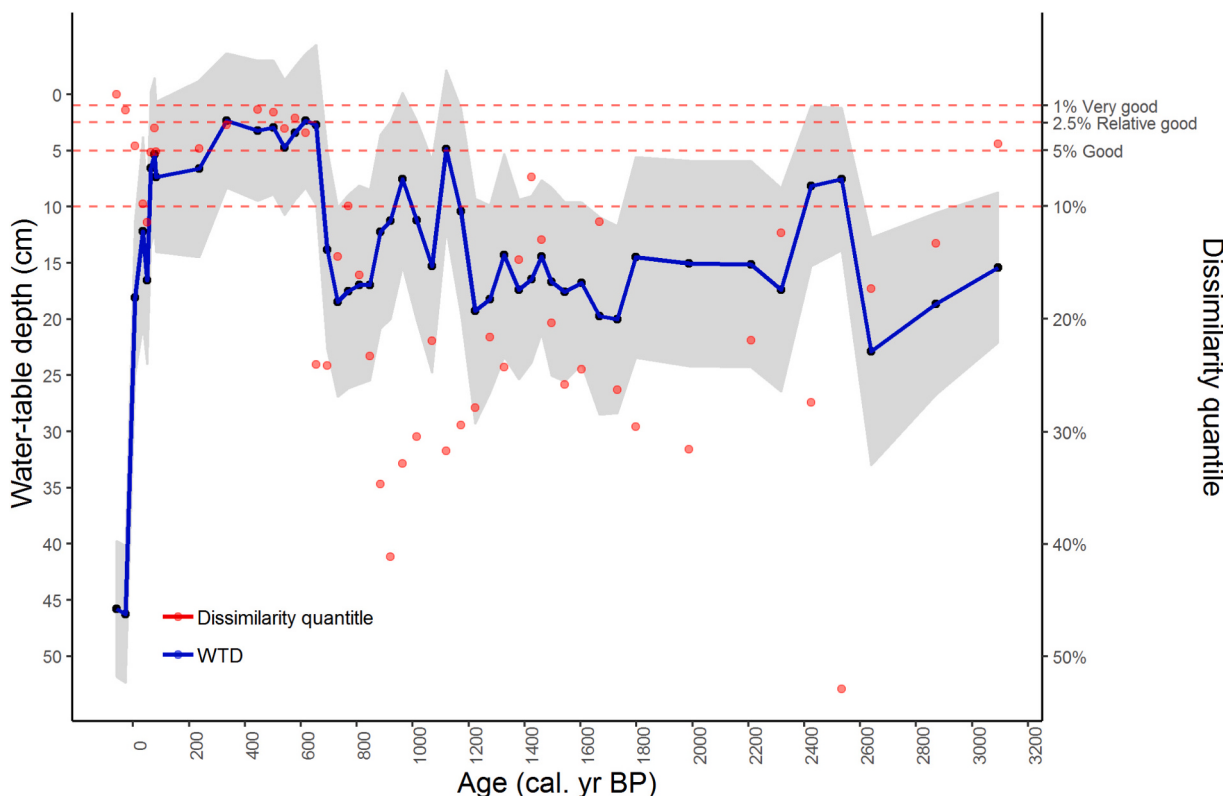


Fig. 5. Reconstructed water table depth (WTD) using the modern analogue technique (MAT) with sample specific error (equivalent to 95 % confidence interval) and dissimilarity quantiles.

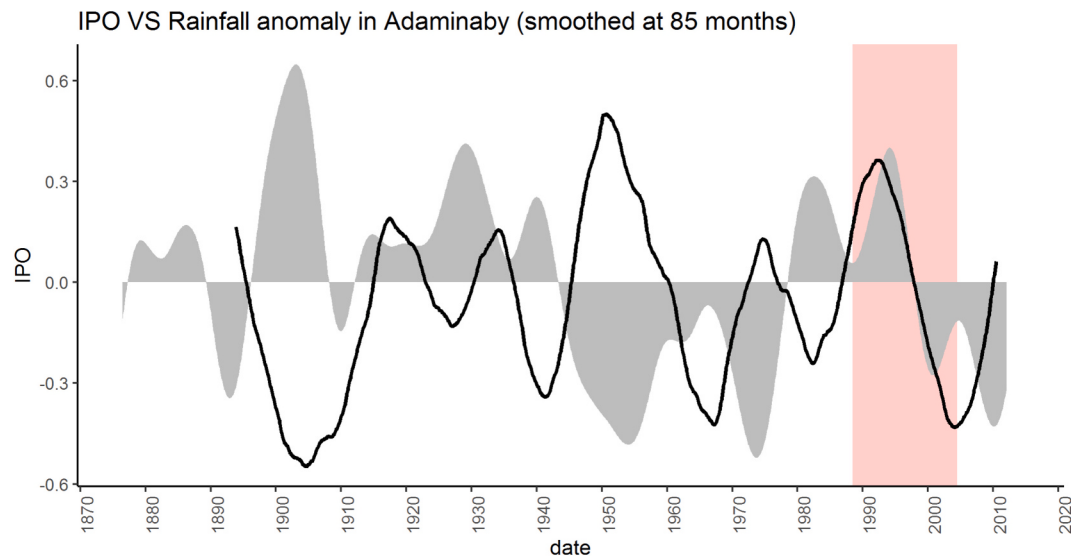


Fig. 6. The correlation between smoothed monthly rainfall in Adaminaby (36° S, 148.77° E, 1015 a.s.l.), south-eastern Australia (in black) and the IPO (filtered TPI, derived from HadISST 1.1 (Henley et al., 2015)) in grey, shaded. The black line was derived by applying an 85-month moving averaging twice on the monthly anomalies, following Dai (2013). The anomalies were obtained by LOESS with span = 0.75 and degree = 2 in R program. The pink bar indicates a shift from a negative correlation before 1988 ($r = -0.53, P < 0.001$) to a positive correlation between 1998 and 2005 ($r = 0.78, p < 0.001$). (For interpretation of the references to colour in this figure legend, the reader is referred to the web version of this article.)

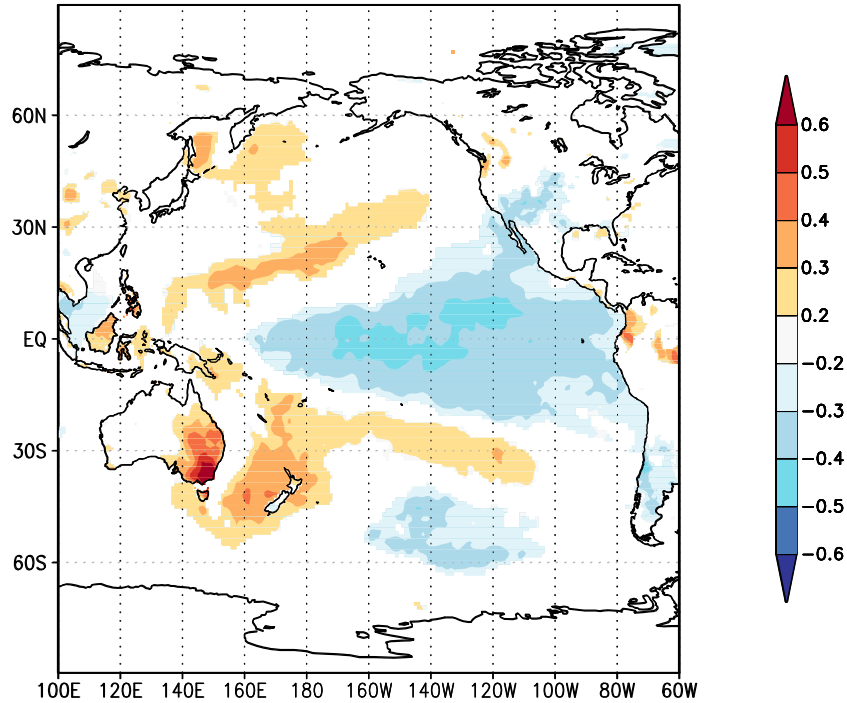


Fig. 7. The correlation of annual rainfall (July–June) in Adaminaby (36° S, 148.77° E, 1015 a.s.l.), south-eastern Australia (Bureau of Meteorology, 2018) with detrended annual sea surface temperature (HadISST 1.1, Rayner et al., 2003) and detrended annual rainfall (CRU TS 4.01, Peterson and Vose, 1997) over the period of 1887 to 1989 in the zone of 100° E and 60° W at 90 % significant level (Created at Climate Explorer <https://climexp.knmi.nl>, November 2018).

Gnotuk (Wilkins et al., 2013). Similarly, the decreasing trend in lake levels from 2.3 to 1.8 ka fit with decreasing water balance at Snowy Flat. The proportion of kaolinite in the Murray Canyons marine sediment core MD03-2611, sampled from offshore South Australia, also implies enhanced fluvial activity at about 2.2 and 1.6 ka (Gingelet al., 2007).

The period of reduced WTD at ~ 920 cal yr at Snowy Flat is evident in the reconstructed rainfall record by Tozer et al. (2016) and in the Morton Bay reconstruction by Coates-Marnane et al. (2018). Cohen et al. (2012) also described an unprecedented fluvial period and high lake

stands at Lake Callabonna in southern central Australia between 900 ± 70 and 850 ± 60 yr B.P.. A brief phase of aeolian dust deposition around 1000 cal yr B.P. at Lake George, implying dry conditions (Fitzsimmons and Barrows, 2010), fits well with the reduction in water balance around ~ 1040 cal yr B.P. at Snowy Flat.

The prolonged period of reduced WTD from 670 and 60 cal yr B.P. is supported by Barr et al. (2014) who inferred a wet period using diatom-derived conductivity at two crater lakes in south-eastern Australia. A trend towards increasing water balance from around 700 cal yr B.P. also

can be seen in the reconstructed western Victorian lake levels (Wilkins et al., 2013) and it is also coincident with relative high lake levels at Lake George in the period between 700 and 300 cal yr B.P. (Fitzsimmons and Barrows, 2010). The period had above average rainfall in the Newcastle reconstruction by Tozer et al. (2016) and the clay content in the Murray Canyons marine sediment core MD03-2611 also implies enhanced fluvial activity (Gingeal et al., 2007). This relatively wetter period is also seemingly evident further afield in Australia: Rouillard et al. (2016) found extreme flooding in arid subtropical north-western Australia during this period and it was a predominantly wet period in the catchment of Moreton Bay in southern Queensland (Coates-Marnane et al., 2018).

The very recent period of increased WTD at Snowy Flat after 60 cal yr B.P. was also evident in other records, with, for example, reduced rainfall in the Williams River catchment (Tozer et al., 2016). It is also supported by Gergis and Henley (2017) who identified more dry anomalies than wet anomalies in south-eastern Australia after 50 cal yr B.P..

4.3. Drivers of late Holocene palaeohydrological variability in south-eastern Australia

In Fig. 8 the reconstruction of WTD at Snowy Flat is compared to several proxies of late Holocene climate. Wilkins et al. (2013) have previously noted that their Holocene reconstruction of lake depth in south-western Victoria displayed a high degree of similarity with the deuterium-derived reconstruction of temperature from the Antarctic EPICA Dome C ice core (Röhlisberger et al., 2004) and this similarity is also apparent here. In Fig. 8 periods of reduced WTD are also closely aligned with low total solar irradiance (TSI), which has been derived from a ^{10}Be record in polar ice (Steinhilber et al., 2009). Notably, the onset of the reduction in WTD at 670 cal yr B.P. at Snowy Flat is also

closely temporally associated with four large volcanic eruptions recorded in the Dome C ice core after 691 B.P. (Miller et al., 2012). These relationships are clearly speculative, given the uncertainties associated with complex and perhaps indirect physical mechanisms linking solar irradiance to WTD changes, especially at centennial to millennial timescales.

In our examination of the instrumental record of rainfall, ENSO also appears to be the primary factor influencing rainfall at an interannual scale, with more rainfall accompanying La Niña, but this relationship is modulated by a negative IPO. These relationships have also previously been described in the rainfall of south-eastern Australia (Power et al., 1998, 1999; Henley et al., 2011; Ashcroft et al., 2016). At a decadal scale, rainfall shows a negative relationship with the IPO (Fig. 6) and rainfall has a statistical relationship with SSTs in the Pacific Ocean and that pattern is clearly an IPO-like ‘tripole’ (Fig. 7). This suggests that rainfall is associated with mean negative IPO (or La Niña-like) states.

In Fig. 8 the reconstruction of WTD is also compared to Rein et al.’s (2005) reconstruction of El Niño based on offshore Peruvian lithic flux. From the base of our Snowy Flat reconstruction of WTD to 1800 cal yr B.P. there are only two peaks and one trough, corresponding to a low frequency of El Niño events. The variability in the reconstructed WTD at Snowy Flat between 1.8 and 0.3 ka coincided with large magnitude El Niño events. Increased WTD at Snowy Flat (consistent with drier, El Niño-like conditions) coincided with frequent El Niño events from 1800 and 1400 cal yr B.P., and the peak in reduced WTD (and surface wetness) around 1720 cal yr B.P. is temporally associated with a reduction in El Niño.

Linking historic precipitation (e.g. Risbey et al., 2009), Holocene climatic variability (e.g. Barr et al., 2014) or fire occurrence (Mariani et al., 2016; Harris and Lucas, 2019) to El Niño event frequency is also a common theme of previous work in south-eastern Australia but other drivers of climatic variability, beyond ENSO, and so including Southern

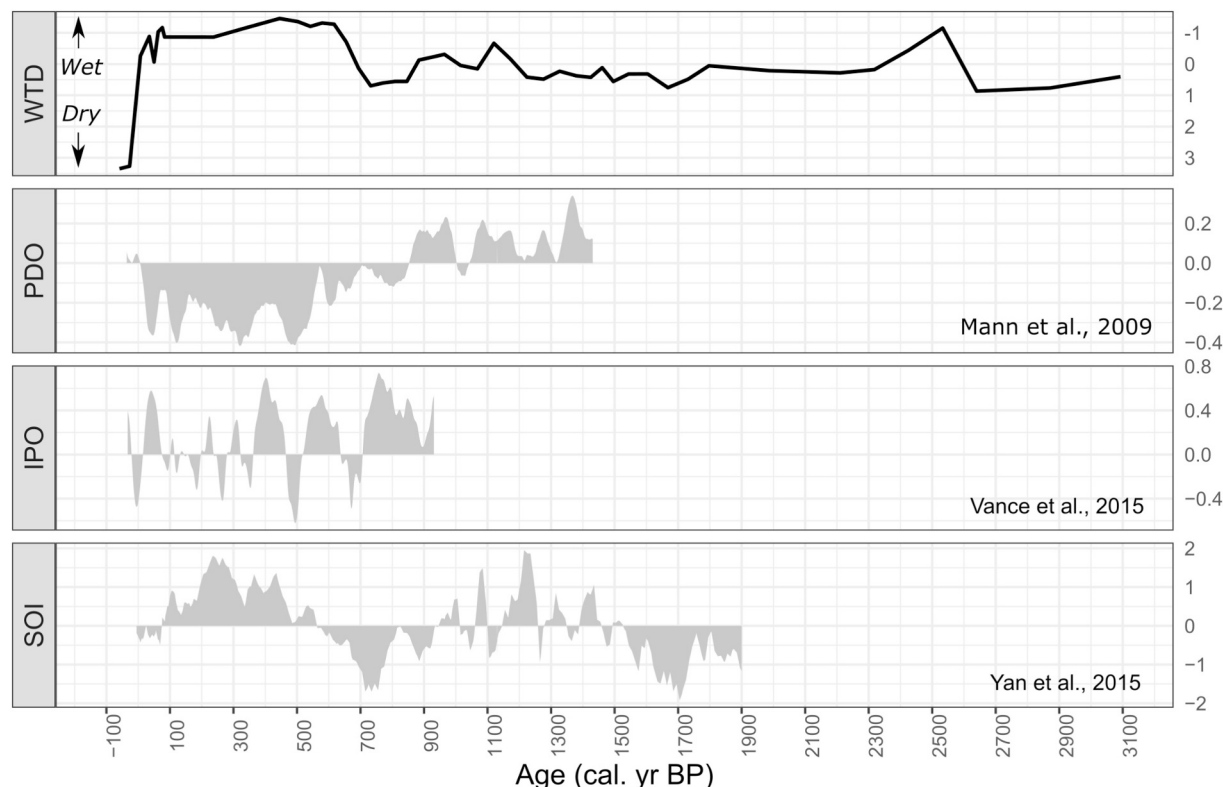


Fig. 8. Comparison of reconstructed water table depth (WTD) at Snowy Flat with reconstructed indices of Pacific Ocean climatic variability. WTD is the z-scored reconstructed water table depth from testate amoebae at Snowy Flat. PDO is the Pacific Decadal Oscillation, derived by Mann et al. (2009) based on global proxy records. IPO is the Interdecadal Pacific Oscillation (with a 40-year moving average) derived by Vance et al. (2015) based on the Antarctic Law Dome ice core record. SOI is a reconstruction of the Southern Oscillation Index by Yan et al. (2015).

Annular Mode (SAM) and the Indian Ocean Dipole (IOD), and their interdependencies (e.g. Abram et al., 2021) must also be considered. Mariani et al. (2016) found a relationship between rainfall (and fire) and SAM in the modern climate of south-western Tasmania, and a relationship at centennial timescales between fire activity and SAM over the last 1000 years. Based on this, it is surprising to find no obvious relationship between the reconstructed DTW at Snowy Flat and the

reconstruction of SAM over the last millennium by Abram et al. (2014).

This relationship between the water table at Snowy Flat and ENSO is further collaborated by the correspondence between trends in our reconstruction and a reconstruction of the SOI by Yan et al. (2011a) (Fig. 9), based on the difference between moisture proxies from the western (Indonesian) and eastern (Galapagos) Pacific. The correspondence with that record includes increased WTD at Snowy Flat from 1950

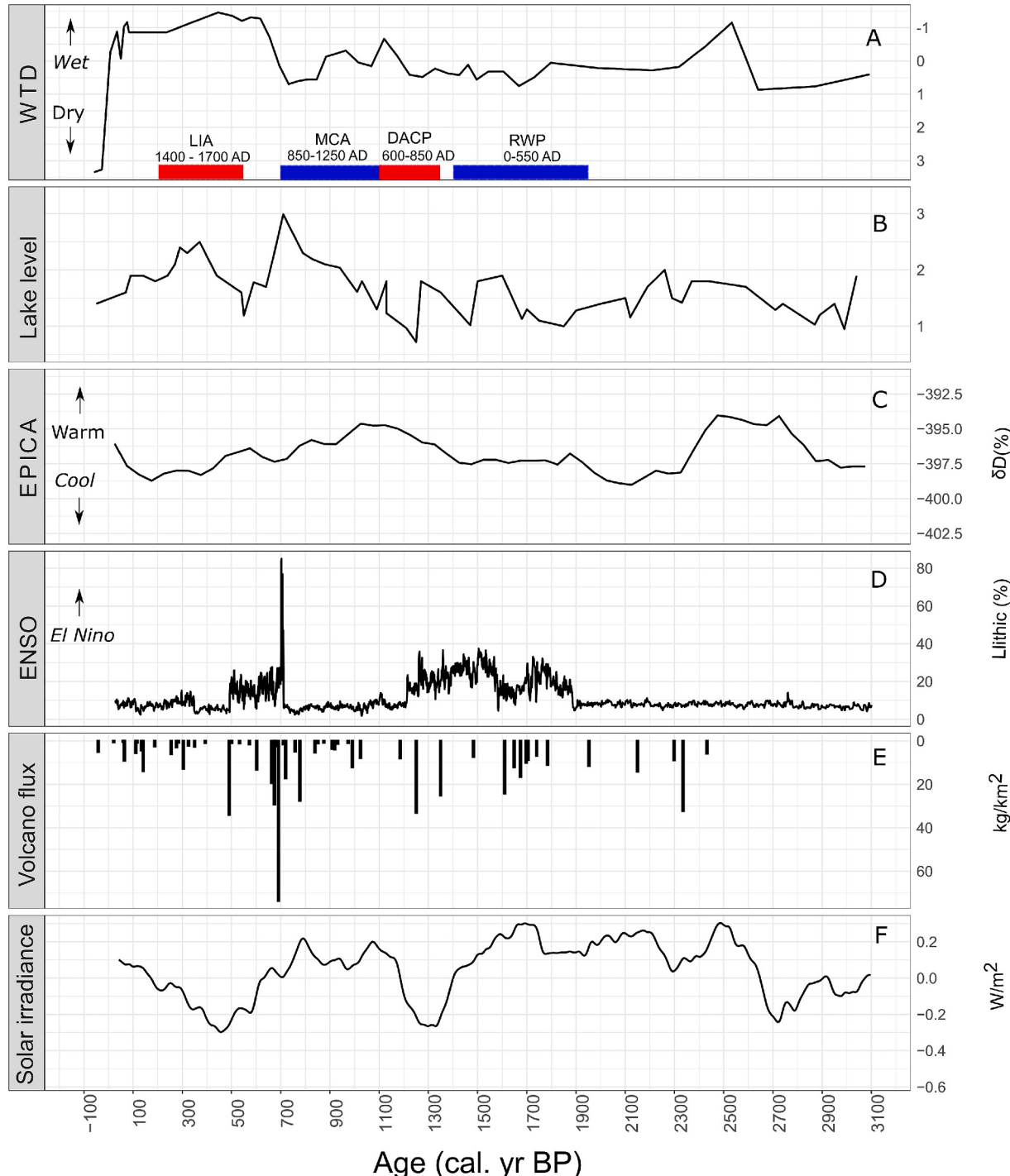


Fig. 9. Comparison of reconstructed water table depth (WTD) at Snowy Flat with paleoenvironmental records. A is the z-scored, reconstructed WTD from testate amoebae at Snowy Flat. This panel also indicates the timing of the Northern Hemisphere historic climate periods including the Roman Warm Period (RWP), the Dark Ages Cold Period (DACP), the Medieval Climatic Anomaly (MCA) and the Little Ice Age (LIA). B is the reconstruction of Victorian lake level by Wilkins et al. (2013). C shows the high resolution EPICA ice core deuterium (δD) record, a proxy for temperature, by Röthlisberger et al. (2004). D is the proxy record of El Niño events based on lithics in an offshore sediment core by Rein et al. (2005). E is a record of volcanics, using sulfate in Dome C ice by Castellano et al. (2005). F is a reconstruction of solar activity based on ^{10}Be in ice cores by Steinhilber et al. (2009).

to 1400 cal yr B.P. which closely corresponds to a period of negative SOI between 1900 and 1500 cal yr B.P. in Yan et al. (2011b) and the increased WTD from 1350 to 1100 cal yr B.P. coincides with a reconstructed positive SOI (Fig. 9).

Reconstructions of the IPO include Vance et al. (2015), based on the concentration of sea salt in the Law Dome ice core from Antarctic which covers the last ~1000 years and Mann et al. (2009) reconstructed the Pacific Decadal Oscillation (PDO) over the last ~1500 years using a global database of proxy records. We compare these to the Snowy Flat reconstruction of WTD in Fig. 9. The Vance et al. (2015) reconstruction of the IPO is consistent with the onset of reduced WTD at Snowy Flat from 670 cal yr B.P. but after that shows higher variability and several transitions between IPO states that are not evident in the Snowy Flat record. The longer Mann et al. (2009) record also has some similarities, but generalisations are difficult. Notably, our inferred wetter surface at Snowy Flat from 670 to 250 cal yr B.P. agrees with the negative PDO derived by Mann et al. (2009).

Solar variation has been associated with widespread climatic anomalies (Lamb, 1965; Eddy, 1976; Bard and Frank, 2006; Steinhilber and Beer, 2011) although the mechanisms (e.g. via stratospheric ozone) are not straightforward (Ball et al., 2016). At Snowy Flat, periods of reduced WTD (and perhaps mean negative IPO states) around 920–860 and 670–60 ca. yr B.P. coincided with the Oort Minima (910–870 B.P.) and a cluster of grand solar minima (including the Wolf Minimum (670–600 B.P.), the Spörer Minimum (490–400 B.P.), the Maunder Minimum (305–235 B.P.) and the Dalton Minimum (160–130 B.P.)), respectively. Meanwhile, the period of increased WTD from 850 to 700 cal yr B.P. coincided with a ~200 year high in solar activity (the Medieval Maximum from 870 to 670 B.P.) which occurred between the Oort and Wolf minima.

These links between solar variability and hydroclimate at the site probably explain why the reconstruction of surface wetness at Snowy Flat includes trends that are reminiscent of broad Northern Hemisphere climatic periods (Fig. 8). At Snowy Flat, increased WTD from 1950 to 1400 cal yr B.P. coincided with the Roman Warming Period (RWP) (Bianchi and McCave, 1999), reduced WTD from 1350 to 1100 cal yr B.P. corresponded to the Dark Ages Cold Period (DACP) (Helama et al., 2017), while increased surface wetness from 1100 to 700 cal yr B.P. occurred within the temporal window associated with Medieval Climatic Anomaly (MCA) (Mann et al., 2009) and enhanced water balance from 670 to 250 cal yr B.P. seems to be temporally associated with the Little Ice Age (LIA) (Mann et al., 2009).

The IPO is thought to be driven by the interaction between tropical and extra-tropical variability, and this generates (negative) feedback at decadal to interdecadal scales (Henley, 2017; England et al., 2014; Farneti et al., 2014; Lu Jr. and Klinger, 1998). The physical mechanism linking the IPO (or the PDO) and the interaction between the tropics and extra-tropical hydroclimate (in places like Snowy Flat) are unclear. A generally dry MCA interspersed by a short, wet period at 920–860 cal yr B.P., associated with a mean positive IPO (or mean El Niño) state, and a wet LIA in south-eastern Australia with a mean negative IPO (or mean La Niña) state are conclusions that agree with Yan et al. (2011b), but contrast with those of Mann et al. (2009) and Goodwin et al. (2014). Notably, Mariani et al. (2016) found no relationship between fire occurrence and the IPO.

As above, it is possible that enhanced surface wetness (reduced WTD, and probably mean negative IPO states) at Snowy Flat and more widely in south-eastern Australia may be associated with low solar irradiance in the late Holocene. This implies negative feedback between radiative forcing and the zonal SST gradient across the equatorial Pacific at decadal-centennial scales. If this is true, it supports the atmospheric hydrological cycle (AHC) (Vecchi et al., 2006; Held and Soden, 2006) rather than the ocean dynamical thermostat (ODT) (Clement et al., 1996) mechanism. The ODT suggests there is positive feedback between warmer temperatures and the zonal SST gradient across the equatorial Pacific, resulting in a La Niña-like mean state. Hence, the MCA has been

associated with a La Niña-like state and the LIA has been described as an El Niño-like state by Mann et al. (2009). In contrast, the AHC mechanism suggests a negative correlation between warming and the zonal SST and sea level pressure gradient across the equatorial Pacific, a weakened Walker Circulation and subsequently an El Niño-like state (Vecchi et al., 2006; Held and Soden, 2006).

The AHC tends to be supported by reconstructions of ENSO that reflect atmospheric (non SST) processes such lake records (Conroy et al., 2008; Sachs et al., 2009; Yan et al., 2011a) and so support for this from the Snowy Flat reconstruction of depth to the water table is not unexpected. It is also possible that the extra-tropical location means that the IPO signal may better reflect a coupled ocean-atmospheric system, which may be different to SST reconstructions which may only capture the oceanic aspect of ENSO. In contrast, the ODT is perhaps better at explaining shorter, interannual, timescales (Vecchi et al., 2006; Collins et al., 2010).

In summary, the Snowy Flat reconstruction of WTD suggests that solar variability leads to changes in Pacific temperature and atmospheric pressure, as reflected in the IPO and hence to rainfall across south-eastern Australia. It should be noted that the mechanisms described above linking solar variability and water balance places an emphasis on rainfall, as a primary determinant. It is also possible that solar variability has a more direct influence on evapotranspiration, for example via temperature, although solar variability and temperature are not well correlated in Antarctica (e.g. cf. Fig. 9 F and C).

It also appears that the onset of the enhanced surface wetness at Snowy Flat at 720 cal yr B.P. happened just after the largest volcanic eruption of the Holocene (Castellano et al., 2005). This volcanic eruption has been associated with the onset of the LIA with cold summers sustained by subsequent sea-ice/ocean feedbacks (Miller et al., 2012). This suggests the period from 720 to 600 cal yr B.P. was a period of transition, probably reflecting the transition of mean background of ENSO or Interdecadal Pacific Oscillation (IPO).

5. Conclusions

This research applied transfer functions between (sub)fossil testate amoebae in peat sediment and water table depth (WTD) at an alpine bog in south-eastern Australia. WTD was derived for the period covering the last 3100 cal yr B.P.. The reconstructed WTD revealed consistent results across several methods, and implied there were periods of enhanced surface wetness around 2480, 1150, 920 and 670–60 cal yr B.P., and increased depth to water table during periods around 2850–2650, 1720, 1040, 860–700 and post 60 cal yr B.P.

Rainfall in many places within south-eastern Australia is strongly associated with La Niña and modulated by negative IPO states (Power et al., 1999; Henley et al., 2011), and so there is more rainfall in a negative IPO state. Consideration of the instrumental record of rainfall from a nearby weather station also confirmed this negative correlation between rainfall and the IPO and revealed an association with an IPO-like tripole pattern in sea surface temperatures in the Pacific Ocean. These suggest that periods of high surface wetness in the Snowy Flat reconstruction might be interpreted as periods of mean negative IPO.

If true, this implies that the IPO was weaker from the base of our analysis at 3100 to 1800 cal yr B.P. and it intensified from 1800 to 250 cal yr B.P.. The reconstructed WTD thus implies that there were several periods of strongly negative IPO states, including 2400–2200, 1350–1100, 920–860 and 670–250 cal yr B.P.. We also suggest a relationship between low total solar irradiance and a negative IPO mean state. Periods of enhanced surface wetness at Snowy Flat around 920–860 and 670–60 cal yr B.P. coincided with solar minima and the period of reduced moisture availability from 850 to 700 cal yr B.P. coincided with the Medieval Maximum.

The reconstruction of WTD at Snowy Flat supports the atmosphere hydrological cycle which provides a mechanism to link radiative forcing and Pacific climatic variability at decadal to centennial timescales. In

contrast, the results do not support the well-accepted ocean dynamical thermostat mechanism for tropical-extratropical links. This research implies a mean negative IPO state during the LIA and a positive IPO mean state in the MCA, and this agrees with atmospheric, rather than SST reconstructions (Yan et al., 2011b).

This is the first application of a testate amoeba-derived index of water table depth in Australia. The derivation of a proxy for water table depth, via transfer functions, represents a significant advantage for regions where lakes are rare or absent, but sediments are accumulating in mires. Further work is likely to unravel the complexities of the drivers of hydroclimatic variability in time and space across south-eastern Australia.

CRediT authorship contribution statement

Xianglin Zheng: Formal analysis, Investigation, Methodology, Writing – original draft. **Geoffrey Hope:** Conceptualization, Funding acquisition, Supervision, Writing – original draft. **Scott D. Mooney:** Conceptualization, Data curation, Formal analysis, Funding acquisition, Investigation, Project administration, Supervision, Writing – original draft, Writing – review & editing.

Declaration of competing interest

The authors declare that they have no known competing financial interests or personal relationships that could have appeared to influence the work reported in this paper.

Acknowledgements

This work is dedicated to the memory of Professor Geoff Hope, who led our investigation of the high-altitude ACT country. We thank the NSW National Parks & Wildlife Service and ACT Parks, Conservation and Lands for facilitating access and sampling in their reserves. We also thank Dr. Benedict Keaney (who collected the upper *Sphagnum* core) and Dr. Len Martin for assistance with field sampling. This research was funded (to SM and GH) by the Temperate Highland Peat Swamps on Sandstone Research Program (THPSS Research Program 2013) administered by the Australian National University. We are grateful for and acknowledge discussion regarding late Holocene climate with Prof Chris Turney and Drs Jonathon Palmer and Zoë Thomas. The careful consideration and comments on a draft version of this manuscript by two anonymous reviewers are gratefully acknowledged.

Data availability

The data associated with this research is available at <https://doi.org/10.26190/unswworks/21130>

References

- Abram, N.J., Mulvaney, R., Vimeux, F., et al., 2014. Evolution of the Southern Annular Mode during the past millennium. *Nat. Clim. Chang.* 4, 564–569.
- Abram, N.J., Henley, B.J., Sen Gupta, A., Lippmann, T.J.R., Clarke, H., Dowdy, A.J., Sharples, J.J., Nolan, R.H., Zhang, T., Wooster, M.J., Wurtzel, J.B., Meissner, K.J., Pitman, A.J., Ukkola, A.M., Murphy, B.P., Tapper, N.J., Boer, M.M., 2021. Connections of climate change and variability to large and extreme forest fires in southeast Australia. *Communications Earth and Environment* 2, 8.
- Amesbury, M.J., Swindles, G.T., Bobrov, A., et al., 2016. Development of a new pan-European testate amoeba transfer function for reconstructing peatland palaeohydrology. *Quaternary Science Reviews* 152, 132–151.
- Ashcroft, L., Gergis, J., Karoly, D.J., 2016. Long-term stationarity of El Niño-Southern Oscillation teleconnections in southeastern Australia. *Climate Dynam.* 46, 2991–3006.
- Ball, W.T., Rozanov, E.V., Alsing, J., Marsh, D.R., Tunmon, F., Mortlock, D.J., Kinnison, D., Haigh, J.D., 2016. The upper stratospheric solar cycle ozone response. *Geophys. Res. Lett.* 46 (3), 1831–1841.
- Bard, E., Frank, M., 2006. Climate change and solar variability: what's new under the Sun? *Earth Planet. Sci. Lett.* 248, 1–14.
- Barr, C., Tibby, J., Gell, P., et al., 2014. Climate variability in South-Eastern Australia over the last 1500 years inferred from the high-resolution diatom records of two crater lakes. *Quaternary Science Reviews* 95, 115–131.
- Bianchi, G.G., McCave, I.N., 1999. Holocene periodicity in North Atlantic climate and deep-ocean flow south of Iceland. *Nature* 397, 515.
- Birks, H.J.B., Lotter, A.F., Juggins, S., et al., 2012. Tracking Environmental Change Using Lake Sediments: Data Handling and Numerical Techniques. Springer Science & Business Media.
- Blaauw, M., Christen, J.A., 2011. Flexible paleoclimate age-depth models using an autoregressive gamma process. *Bayesian Anal.* 6, 457–474.
- BOM, 2018a. Mount Ginini AWS (site no. 070349) Summary Statistics. Bureau of Meteorology, Australian Government. Available at [http://www.bom.gov.au/jsp/ncc/cdio/weatherData/av?p_nccObsCode=136&p_display_type=dailyDataFile&p_stn_num=070349&p_startYear=](http://www.bom.gov.au/jsp/ncc/cdio/wData/wdata?p_nccObsCode=136&p_display_type=dailyDataFile&p_stn_num=070349&p_startYear=), accessed Nov., 2018.
- BOM, 2018b. Adaminaby Alpine Tourist Park (site no. 071000) Summary Statistics. Bureau of Meteorology, Australian Government. Available at http://www.bom.gov.au/jsp/ncc/cdio/weatherData/av?p_nccObsCode=136&p_display_type=dailyDataFile&p_stn_num=71000. accessed Nov., 2018.
- Booth, R., Lamontowicz, M., Charman, D., 2010. Preparation and analysis of testate amoebae in peatland paleoenvironmental studies. *Mires and Peat* 7, Article 2.
- Bowler, J.M., 1981. Australian salt lakes. Springer, Salt lakes, pp. 431–444.
- Castellano, E., Becagli, S., Hansson, M., et al., 2005. Holocene volcanic history as recorded in the sulfate stratigraphy of the European Project for Ice Coring in Antarctica Dome C (EDC96) ice core. *J. Geophys. Res. Atmos.* 110, D06114.
- Chang, J.C., Woodward, C., Shulmeister, J., 2014. A snapshot of the limnology of eastern Australian water bodies spanning the tropics to Tasmania: the land-use, climate, limnology nexus. *Mar. Freshw. Res.* 65, 872–883.
- Charman, D.J., Hendon, D., Woodland, W.A., 2000. The Identification of Testate Amoebea (Protozoa: Rhizopoda) in Peats. Technical Guide No. 9. Quaternary Research Association, Great Britain.
- Charman, D.J., Blundell, A., Chiverrell, R.C., et al., 2006. Compilation of non-annually resolved Holocene proxy climate records: stacked Holocene peatland paleo-water table reconstructions from northern Britain. *Quat. Sci. Rev.* 25, 336–350.
- Clark, R., 1980. Sphagnum Growth on Ginini Flats, ACT. Unpublished Report to NSW National Parks and Wildlife Service.
- Clement, A.C., Seager, R., Cane, M.A., et al., 1996. An ocean dynamical thermostat. *J. Climate* 9, 2190–2196.
- Coates-Marnane, J., Olley, J., Tibby, J., et al., 2018. A 1500 year record of river discharge inferred from fluvial-marine sediments in the Australian subtropics. *Palaeogeography, Palaeoclimatology, Palaeoecology* 504, 136–149.
- Cohen, T.J., Nanson, G.C., 2007. Mind the gap: an absence of valley-fill deposits identifying the Holocene hypsithermal period of enhanced flow regime in southeastern Australia. *The Holocene* 17, 411–418.
- Cohen, T.J., Nanson, G.C., Jansen, J.D., et al., 2012. A pluvial episode identified in arid Australia during the medieval Climatic Anomaly. *Quaternary Science Reviews* 56, 167–171.
- Collins, M., An, S.-I., Cai, W., et al., 2010. The impact of global warming on the tropical Pacific Ocean and El Niño. *Nat. Geosci.* 3, 391.
- Conroy, J.L., Overpeck, J.T., Cole, J.E., et al., 2008. Holocene changes in eastern tropical Pacific climate inferred from a Galápagos lake sediment record. *Quaternary Science Reviews* 27, 1166–1180.
- Dai, A., 2013. The influence of the inter-decadal Pacific oscillation on US precipitation during 1923–2010. *Climate Dynam.* 41, 633–646.
- Dodson, J.R., 1987. Mire development and environmental change, Barrington Tops, New South Wales, Australia. *Quatern. Res.* 27, 73–81.
- Eddy, J.A., 1976. The Maunder Minimum. *Science* 192, 1189–1202.
- England, M.H., McGregor, S., Spence, P., et al., 2014. Recent intensification of wind-driven circulation in the Pacific and the ongoing warming hiatus. *Nature Climate Change* 4, 222–227.
- Farneti, R., Molteni, F., Kucharski, F., 2014. Pacific interdecadal variability driven by tropical-extratropical interactions. *Climate Dynam.* 42, 3337–3355.
- Fitzsimmons, K.E., Barrows, T.T., 2010. Holocene hydrologic variability in temperate southeastern Australia: An example from Lake George, New South Wales. *The Holocene* 20, 585–597.
- Gergis, J., Henley, B.J., 2017. Southern Hemisphere rainfall variability over the past 200 years. *Climate Dynam.* 48, 2087–2105.
- Ginge, F., De Deckker, P., Norman, M., 2007. Late Pleistocene and Holocene climate of SE Australia reconstructed from dust and river loads deposited offshore the River Murray Mouth. *Earth Planet. Sci. Lett.* 255, 257–272.
- Goodwin, I.D., Browning, S., Lorrey, A.M., et al., 2014. A reconstruction of extratropical Indo-Pacific sea-level pressure patterns during the medieval climate Anomaly. *Climate Dynam.* 43, 1197–1219.
- Gore, A., 1983. Ecosystems of the World. Mires: Swamp, Bog, Fen and Moor. Elsevier, Amsterdam, The Netherlands.
- Gouramanis, C., De Deckker, P., Switzer, A.D., et al., 2013. Cross-continent comparison of high-resolution Holocene climate records from southern Australia — Deciphering the impacts of far-field teleconnections. *Earth Sci. Rev.* 121, 55–72.
- Harris, S., Lucas, C., 2019. Understanding the variability of Australian fire weather between 1973 and 2017. *PloS One* 14, e0222328.
- Heinrich, I., Allen, K., 2013. Current issues and recent advances in Australian dendrochronology: where to next? *Geogr. Res.* 51, 180–191.
- Helama, S., Jones, P.D., Briffa, K.R., 2017. Dark Ages Cold Period: A literature review and directions for future research. *The Holocene* 27, 1600–1606.
- Held, I.M., Soden, B.J., 2006. Robust responses of the hydrological cycle to global warming. *J. Climate* 19, 5686–5699.

- Henley, B.J., 2017. Pacific decadal climate variability: Indices, patterns and tropical-extratropical interactions. *Global Planet. Change* 155, 42–55.
- Henley, B.J., Thyer, M.A., Kuczera, G., et al., 2011. Climate-informed stochastic hydrological modelling: Incorporating decadal-scale variability using paleo data. *Water Resour. Res.* 47, W11509.
- Henley, B.J., Gergis, J., Karoly, D.J., et al., 2015. A Tripole Index for the Interdecadal Pacific Oscillation. *Climate Dynam.* 45, 3077–3090.
- Hogg, A.G., Hua, Q., Blackwell, P.G., et al., 2013. SHCal13 Southern Hemisphere calibration, 0–50,000 years cal BP. *Radiocarbon* 55, 1889–1903.
- Hope, G., 2003. The mountain mires of southern New South Wales and the Australian Capital Territory: Their history and future. In: Mackay, J., Associates (Eds.), *Proceedings of an International Year of the Mountains Conference, Jindabyne Nov 25–28, 2002*. Australian Alps Liaison Committee, Canberra, pp. 67–79.
- Hope, G., Nanson, R., Flett, I., 2009. The Peat-Forming Mires of the Australian Capital Territory. Technical Report 19. Territory and Municipal Services, Canberra, Australia.
- Hua, W., Dai, A., Qin, M., 2018. Contributions of Internal Variability and External Forcing to the Recent Pacific Decadal Variations. *Geophys. Res. Lett.* 45, 7084–7092.
- Jansen, E., Overpeck, J., Briffa, K., et al., 2007. Palaeoclimate. In: *Climate Change 2007: The Physical Science Basis*. Contribution of Working Group I to the Fourth Assessment Report of the Intergovernmental Panel on Climate Change. S. Solomon, D. Qin, M. Manning, et al. (Eds.). Cambridge University Press, pp. 433–497.
- Jowsey, P.C., 1966. An improved peat sampler. *New Phytol.* 65, 245–248.
- Juggins, S., 2017. rioja: Analysis of Quaternary Science Data, R package version (0.9-15).
- Lamb, H.H., 1965. The early medieval warm epoch and its sequel. *Palaeogeogr. Palaeoclimatol. Palaeoecol.* 1, 13–37.
- Lu Jr., P., Klinger, B.A., 1998. Meridional Circulation Cells and the Source Waters of the Pacific Equatorial Undercurrent. *J. Phys. Oceanogr.* 28, 62–84.
- Macphail, M.K., Hope, G.S., 1985. Late Holocene mire development in montane southeastern Australia: a sensitive climatic indicator. *Search* 15, 344–348.
- Mann, M.E., Zhang, Z., Rutherford, S., et al., 2009. Global signatures and dynamical origins of the Little Ice Age and medieval climate Anomaly. *Science* 326, 1256–1260.
- Mariotti M, Fletcher MS, Holz A and Nyman P (2016) ENSO controls interannual fire activity in Southeast Australia. *Geophys. Res. Lett.* 43 (20), 10,891–10,900.
- McKeown, M.M., Burge, O.R., Richardson, S.J., Wood, J.R., Mitchell, E.A.D., Wilmshurst, J.M., 2024. Biomonitoring tool for New Zealand peatlands: Testate amoebae and vascular plants as promising bioindicators. *J. Environ. Manage.* 354, 120.
- Mieczan, T., Adamczuk, M., 2015. Ecology of testate amoebae (Protists) in mosses: distribution and relation of species assemblages with environmental parameters (King George Island, Antarctica). *Polar Biol.* 38, 221–230.
- Miller, G.H., Geirsdóttir, Á., Zhong, Y., et al., 2012. Abrupt onset of the Little Ice Age triggered by volcanism and sustained by sea-ice/ocean feedbacks. *Geophys. Res. Lett.* 39, L02708.
- Mitchell, E.A.D., Charman, D.J., Warner, B.G., 2008. Testate amoebae analysis in ecological and paleoecological studies of wetlands: past, present and future. *Biodivers. Conserv.* 17, 2115–2137.
- Muller, R., Nicholson, A., Wooldridge, A., et al., 2016. Hydrogeological Landscapes of the Australian Capital Territory. Office of Environment and Heritage: Wagga Wagga, NSW, Australia.
- Neukom, R., Gergis, J., 2012. Southern Hemisphere high-resolution palaeoclimate records of the last 2000 years. *The Holocene* 22, 501–524.
- Oksanen, J., Kindt, R., Legendre, P., et al., 2015. vegan: Community Ecology Package. R package version 2.2-1.
- PAGES 2k Consortium, 2013. Continental-scale temperature variability during the past two millennia. *Nat. Geosci.* 6, 339–346.
- Palmer, J.G., Cook, E.R., Turney, C.S., et al., 2015. Drought variability in the eastern Australia and New Zealand summer drought atlas (ANZDA, CE 1500–2012) modulated by the Interdecadal Pacific Oscillation. *Environ. Res. Lett.* 10, 124002.
- Payne, R.J., Mitchell, E.A.D., 2009. How many is enough? Determining optimal count totals for ecological and palaeoecological studies of testate amoebae. *J. Paleolimnol.* 42, 483–495.
- Peterson, T.C., Vose, R.S., 1997. An overview of the Global Historical Climatology Network temperature database. *Bull. Am. Meteorol. Soc.* 78, 2837–2850.
- Petherick, L., Bostock, H., Cohen, T.J., et al., 2013. Climatic records over the past 30 ka from temperate Australia - a synthesis from the Oz-INTIMATE workgroup. *Quaternary Science Reviews* 74, 58–77.
- Power, S., Tseitkin, F., Torok, S., et al., 1998. Australian temperature, Australian rainfall and the Southern Oscillation, 1910–1992: coherent variability and recent changes. *Aust. Met. Mag.* 47, 85–101.
- Power, S., Casey, T., Folland, C., et al., 1999. Inter-decadal modulation of the impact of ENSO on Australia. *Climate Dynam.* 15, 319–324.
- Rayner, N., Parker, D.E., Horton, E., et al., 2003. Global analyses of sea surface temperature, sea ice, and night marine air temperature since the late nineteenth century. *J. Geophys. Res. Atmos.* 108, 4407.
- Rein, B., Lückge, A., Reinhardt, L., et al., 2005. El Niño variability off Peru during the last 20,000 years. *Paleoceanography* 20, PA4003.
- Risbey, J.S., Pook, M.J., McIntosh, P.C., et al., 2009. On the remote drivers of rainfall variability in Australia. *Mon. Weather Rev.* 137, 3233–3253.
- Röthlisberger, R., Bigler, M., Wolff, E.W., Joos, F., Monnin, Hutterli, M.A., 2004. Ice core evidence for the extent of past atmospheric CO₂ change due to iron fertilisation. *Geophys. Res. Lett.* 31, L16207. <https://doi.org/10.1029/2004GL020338>.
- Rouillard, A., Skrzypek, G., Turney, C., et al., 2016. Evidence for extreme floods in arid subtropical Northwest Australia during the Little Ice Age chronozone (CE 1400–1850). *Quaternary Science Reviews* 144, 107–122.
- Sachs, J.P., Sachse, D., Smittenberg, R.H., et al., 2009. Southward movement of the Pacific intertropical convergence zone AD1400–1850. *Nat. Geosci.* 2, 519.
- Steinhilber, F., Beer, J., 2011. Solar activity—the past 1200 years. *PAGES News* 19, 5–6.
- Steinhilber, F., Beer, J., Fröhlich, C., 2009. Total solar irradiance during the Holocene. *Geophys. Res. Lett.* 36, L19704.
- Sullivan, M., Booth, R., 2007. Key of Testate Amoebae Inhabiting Sphagnum-Dominated Peatlands with an Emphasis on Taxa Preserved in Holocene Sediments. Lehigh University, Bethlehem.
- Swindles, G.T., Holden, J., Raby, C.L., et al., 2015. Testing peatland water-table depth transfer functions using high-resolution hydrological monitoring data. *Quaternary Science Reviews* 120, 107–117.
- Tibby, J., 2003. Explaining lake and catchment change using sediment derived and written histories: an Australian perspective. *Sci. Total Environ.* 310, 61–71.
- Timmermann, A., An, S.-I., Kug, J.-S., et al., 2018. El Niño–Southern Oscillation complexity. *Nature* 559, 535–545.
- Tozer, C.R., Vance, T.R., Roberts, J.L., et al., 2016. An ice core derived 1013-year catchment-scale annual rainfall reconstruction in subtropical eastern Australia. *Hydrolog. Earth Syst. Sci.* 20, 1703–1717.
- van Bellen, S., Mauquoy, D., Payne, R.J., Roland, T.P., Daley, T.J., Hughes, P.D.M., Loader, N.J., Street-Perrott, F.A., Rice, E.M., Pancotto, V.A., 2014. Testate amoebae as a proxy for reconstructing Holocene water table dynamics in southern Patagonian peat bogs. *J. Quat. Sci.* 29, 463–474.
- van Oldenborgh, G.J., Burgers, G., 2005. Searching for decadal variations in ENSO precipitation teleconnections. *Geophys. Res. Lett.* 32 (15), 1–5. <https://doi.org/10.1029/2005GL023110>.
- Vance, T.R., Roberts, J.L., Plummer, C.T., et al., 2015. Interdecadal Pacific variability and eastern Australian megadroughts over the last millennium. *Geophys. Res. Lett.* 42, 129–137.
- Vecchi, G.A., Soden, B.J., Wittenberg, A.T., et al., 2006. Weakening of tropical Pacific atmospheric circulation due to anthropogenic forcing. *Nature* 441, 73.
- Wanner, H., Mercalli, L., Grosjean, M., et al., 2015. Holocene climate variability and change: a data-based review. *J. Geol. Soc. London* 172, 254–263.
- Warner, B.G., Charman, D.J., 1994. Holocene changes on a peatland in northwestern Ontario interpreted from testate amoebas (Protozoa) analysis. *Boreas* 23, 270–279.
- Whinam, J., Hope, G., 2005. The peatlands of the Australasian region. In: Moore - von Sibirien bis Feuerland (Mires - from Siberia to Tierra del Fuego) (1st Ed., Vol. 1, pp. 397–434). Biologiezentrum der Oberösterreichischen Landesmuseen. Available at https://www.zobodat.at/pdf/STAPFIA_0085_0397-0433.pdf. accessed March 2025.
- Wickham, H., 2009. R Package: ggplot2: Elegant Graphics for Data Analysis.
- Wilkins, D., Gouramanis, C., De Deckker, P., et al., 2013. Holocene lake-level fluctuations in Lakes Keilambete and Gnotuk, southwestern Victoria, Australia. *The Holocene* 23, 784–795.
- Yan, H., Sun, L., Wang, Y., et al., 2011a. A record of the Southern Oscillation Index for the past 2,000 years from precipitation proxies. *Nat. Geosci.* 4, 611.
- Yan, H., Sun, L., Oppo, D.W., et al., 2011b. South China Sea hydrological changes and Pacific Walker Circulation variations over the last millennium. *Nat. Commun.* 2, 293.
- Yeh, S.-W., Wang, X., Wang, C., et al., 2015. On the Relationship between the North Pacific climate Variability and the Central Pacific El Niño. *J. Climate* 28, 663–677.
- Yu, J.-Y., Lu, M.-M., Kim, S.T., 2012. A change in the relationship between tropical Central Pacific SST variability and the extratropical atmosphere around 1990. *Environ. Res. Lett.* 7, 034025.
- Zheng, X., 2018. The reconstruction of moisture availability in south-eastern Australia during the Holocene. PhD Thesis. School of Biological, Earth & Environmental Sciences, University of New South Wales, Sydney, Australia. <https://doi.org/10.26190/unswworks/21130>. available at.
- Zheng, X., Amesbury, M.J., Hope, G., Martin, L.F., Mooney, S.D., 2019a. Testate amoebae as a hydrological proxy for reconstructing water table depth in the mires of south-eastern Australia. *Ecol. Indic.* 96, 701–710.
- Zheng, X., Harper, B.J., Hope, G., Mooney, S.D., 2019b. A new preparation method for testate amoebae in mineralogenic sediments. *Mires and Peat* 29, 1–12. <https://doi.org/10.19189/MaP.2018.OMB.380>. Article 30.
- Zheng, X., Hope, G., Mooney, S.D., 2025. Snowy flat bog, ACT palaeohydrology and palaeoenvironmental data. Dataset UNSWorks. <http://hdl.handle.net/1959.4/104470> (accessed August, 2025).